Radiation Measurements 85 (2016) 126–133

Contents lists available at ScienceDirect

Radiation Measurements

journal homepage: www.elsevier.com/locate/radmeas

Simulated minimum detectable activity concentration (MDAC) for a real-time UAV airborne radioactivity monitoring system with HPGe and $LaBr_3$ detectors

Xiao-Bin Tang [a, b, *], Jia Meng [a], Peng Wang [a], Ye Cao [a], Xi Huang [a], Liang-Sheng Wen [a], Da Chen [a, b]

[a] Department of Nuclear Science and Engineering, Nanjing University of Aeronautics and Astronautics, Nanjing 210016, China
[b] Jiangsu Key Laboratory of Nuclear Energy Equipment Materials Engineering, Nanjing University of Aeronautics and Astronautics, Nanjing 210016, China

HIGHLIGHTS

- A real-time UAV airborne radioactivity monitoring system (NH-UAV) was developed.
- The efficiency calculations and MDAC values are given.
- NH-UAV is able to monitor major nuclear accidents, such as the Fukushima accident.
- The source term size can influence the detection sensitivity of the system.
- The HPGe detector possesses measurement thresholds on activity concentration.

ARTICLE INFO

Article history:
Received 28 April 2015
Received in revised form
2 December 2015
Accepted 26 December 2015
Available online 29 December 2015

Keywords:
Nuclear accident
Minimum detectable activity concentration
Monte Carlo simulation
HPGe detector
$LaBr_3$ detector

ABSTRACT

An automatic real-time UAV airborne radioactivity monitoring system with high-purity germanium (HPGe) and lanthanum bromide ($LaBr_3$) detectors (NH-UAV) was developed to precisely obtain small-scope nuclide information in major nuclear accidents. The specific minimum detectable activity concentration (MDAC) calculation method for NH-UAV in the atmospheric environment was deduced in this study for a priori evaluation and quantification of the suitability of NH-UAV in the Fukushima nuclear accident, where the MDAC values of this new equipment were calculated based on Monte Carlo simulation. The effects of radioactive source term size and activity concentration on the MDAC values were analyzed to assess the detection performance of NH-UAV in more realistic environments. Finally, the MDAC values were calculated at different shielding thicknesses of the HPGe detector to improve the detection capabilities of the HPGe detector, and the relationship between the MDAC and the acquisition time of the system was deduced. The MDAC calculation method and data results in this study may be used as a reference for in-situ radioactivity measurement of NH-UAV.

1. Introduction

The unmanned aerial vehicle (UAV) aviation radiation monitoring system has numerous advantages, such as quick response, unlimited traffic conditions, and substantial reductions in radiation hazards for operators. Many research studies on UAV aviation radiation monitoring system have been conducted in recent years (Kurvinen et al., 2005; Pöllänen et al., 2009; Peräjärvi et al., 2008; Castelluccio et al., 2012; Airborne pods seek to tra; Lee et al., 2009; MacFarlane et al., 2014; Sanada and Torii, 2015). Among these studies, some UAVs are equipped with sampling systems. For example, the Finnish group has designed an aerial radioactivity monitoring system with a detector and a sampler (Kurvinen et al., 2005; Pöllänen et al., 2009; Peräjärvi et al., 2008). The Italian Institute of Health has developed an aerial platform equipped with a compact air sampling line and a complex of detectors for real time measurements (Castelluccio et al., 2012). Detection systems equipped with sampler are relatively complicated, and it is more difficult to determine the detection performance, such as MDAC.

* Corresponding author. Department of Nuclear Science and Engineering, Nanjing University of Aeronautics and Astronautics, Nanjing 210016, China.
E-mail address: tangxiaobin@nuaa.edu.cn (X.-B. Tang).

http://dx.doi.org/10.1016/j.radmeas.2015.12.031
1350-4487/

Besides, radioactive monitoring in major nuclear accidents is a demanding task because of various radionuclides and complex source terms. In particular, radioactivity in the distance superimposes on the detection spectrum, leading to considerable deviation in detection results. Thus, further research is necessary.

In this study, a UAV airborne radioactivity monitoring equipment based on a double detector system called "NH-UAV" was developed in Interdisciplinary InnoCentre for Nuclear Technology (IINT) in Nanjing University of Aeronautics and Astronautics (NUAA) to realize air radiation monitoring under major nuclear accidents. In the developed equipment, high-purity germanium (HPGe) and lanthanum bromide ($LaBr_3$) detectors could back up, supply, and verify the detection data of the other. Thus, the reliability of detection results was improved.

Minimum detectable activity concentration (MDAC) denotes the minimum amount of activity that a detection system can detect reliably (with a confidence limit of 95%) (Currie, 1968). The applicability of the newly developed monitoring equipment in a radioactive environment should be predicted. Meanwhile, for radionuclides, being detected by detectors is the prerequisite to be analyzed and processed. Thus, calculating the MDAC value of the new NH-UAV device is essential. However, in contrast to conventional detection on land, the radioactivity measurement of NH-UAV in air under major nuclear accidents is a type of volumetric source detection and then has the different definition and calculation method on the background and detection efficiency, for the background of the HPGe detector is volumetric source and the detection efficiency of the $LaBr_3$ detector is volumetric efficiency (Zhang et al., 2015). Therefore, the general MDAC calculation method is not completely suitable for NH-UAV.

The MDAC of this particular device in the Fukushima nuclear accident was calculated in this study based on the Monte Carlo (MC) method to evaluate the detection performance of NH-UAV in major accidents. Given the uncertainty of radiation leakage, the source term size and activity concentration were important factors that affected the detection capability of the detection system; hence, the MDAC of NH-UAV was studied on these two sides. Moreover, the measurement capabilities of this monitoring system were discussed with different acquisition time and shielding thicknesses of the HPGe detector.

2. Materials and methods

2.1. Description of the double detector system

The double detector system is the core unit of NH-UAV, comprising an HPGe semiconductor detector and a $LaBr_3$ scintillator detector. As shown in Fig. 1, B represents the $LaBr_3$ scintillator detector, whose probe is directly exposed to air, monitoring a wide range of radioactivity, including radioactive gases and radioactive aerosols. However, considerable deviations occur because of the radioactivity in the distance superimposes on the detection spectrum. C denotes the HPGe detector with wolfram collimator (1 cm), whose probe has a filter at the front, detecting the radioactivity adsorbed on the filter to precisely obtain small-scope nuclide information of radioactive aerosols. Because of the shielding in the device, the radioactive gases cannot be detected.

To obtain precise nuclide information, the detection data of the HPGe and $LaBr_3$ detectors should be corrected. A certain algorithm is utilized to validate, supply, and optimize the detection data to achieve the nuclide identification and activity concentrations of radioactive nuclides within a small scope (Cao et al., 2015).

In general, the process of radioactivity measurement of the HPGe detector consists of three steps. Firstly, the air flow enters from the air inlet (H) and goes out through the air exhaust (F), and

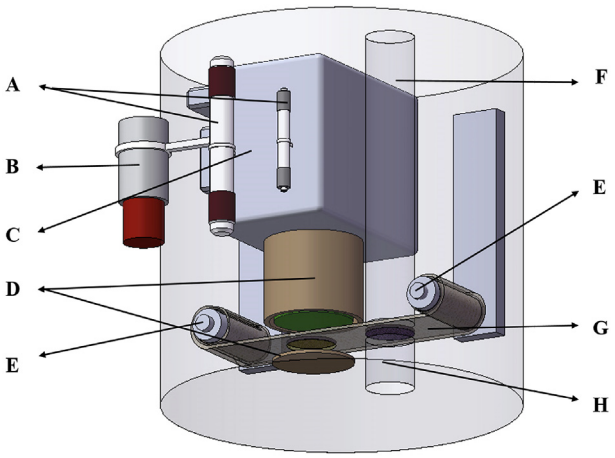

Fig. 1. General scheme of the double detector system: A: GM counters, B: $LaBr_3$ scintillator detector, C: HPGe semiconductor detector, D: collimator of HPGe detector, E: motorized roller, F: air exhaust, G: filter membrane, H: air inlet.

then the radioactive aerosols are deposited on the filter membrane (G). Secondly, the filter membrane (with the radioactive aerosols) is transmitted by the motorized roller (E) to the HPGe probe (C) to be detected. Finally, the measured data is first framed with data transmission and then transmitted to the PC on the ground.

The HPGe gamma spectrometer (model trans-SPEC-DX-100T) is an ORTEC GEM Series P-type crystal (65 mm in diameter and 50 mm in length), its nominal relative efficiency is 40% and the FWHM at 1332 keV is approximately 2.3 keV. The $LaBr_3$ detector (Saint-Gobain) is a cylindrical crystal (38.1 mm × 38.1 mm) with 12% relative efficiency and the FWHM at 662 keV is approximately 29 keV.

2.2. Efficiency of the double detector system

Determining the efficiency of the double detector system is essential to NH-UAV for radioactivity measurement in the air. The detection efficiency of NH-UAV is composed of two parts.

The efficiency of the HPGe detector can be converted to the volumetric detection efficiency ε_H [(Bq m^{-3})$^{-1}$]:

$$\varepsilon_H = \varepsilon \cdot V_H \cdot P. \tag{1}$$

The volumetric efficiency ε_L [(Bq m^{-3})$^{-1}$] of the $LaBr_3$ detector is:

$$\varepsilon_L = \varepsilon \cdot V_L, \tag{2}$$

where ε is the photopeak efficiency at a specific energy, V_H (m^3) is the air volume through the filter during the sampling time, P is the filter adsorption efficiency (50%), and V_L (m^3) is the air volume for each γ-ray.

Then, the activity concentration A_X is expressed as follows (Khan et al., 2008):

$$A_X = \frac{N}{\varepsilon_X \cdot T_L \cdot I_\gamma}, \tag{3}$$

where A_X can be either the activity concentration A_H (Bq m^{-3}) of radioactive aerosols detected by the HPGe detector in a small area or the activity concentration A_L (Bq m^{-3}) of radioactive aerosols and radioactive gases detected by the $LaBr_3$ detector in a broad region; N is the counts under the peak; T_L is the acquisition time (10 s); I_γ is the emission probability of the γ-ray; and ε_X can be either the

detection efficiency ε_H of the HPGe detector or the detection efficiency ε_L of the $LaBr_3$ detector.

2.3. MDAC of the double detector system

MDAC can be used to denote the detection capability of the detection systems, signifying the minimum amount of a nuclide that the detection systems can analyze in a specific confidence degree (with a confidence limit of 95%) and application. A γ-ray at a specific energy can be detected reliably by the detection system if its activity concentration is larger than the corresponding MDAC value.

The MDAC of NH-UAV comprises two parts: one is the MDAC of radioactive aerosols detected by the HPGe detector, and the other is the MDAC of radioactive aerosols and gases detected by the $LaBr_3$ detector.

Given that the background of the HPGe detector is the radiation passing through the shield, which is closely related to the source term size and activity concentration, and the $LaBr_3$ detector efficiency is the volumetric source efficiency, which also closely related to the source term size. Therefore, the MDAC of NH-UAV has a specific calculation method.

After the efficiency calibration, the MDAC (with a confidence limit of 95%) of NH-UAV can be calculated by Gong et al. (2014), Bento et al. (2010), Casanovas et al. (2014a):

$$MDAC_X = \frac{L_D}{\varepsilon_X \cdot T_L \cdot I_\gamma}, \tag{4}$$

where $MDAC_X$ can be either $MDAC_H$ of the HPGe detector or $MDAC_L$ of the $LaBr_3$ detector and L_D is the detection limit.

L_D (with a confidence limit of 95%) for a certain Region of Interest (ROI) can be given as:

$$L_D = 2.71 + 4.65\sqrt{B_x}, \tag{5}$$

where B_X can be the background B_H of the HPGe detector or the background B_L of the $LaBr_3$ detector in the considered ROI.

The width of the ROI is proportional to the *FWHM(E)* function of each detector (Casanovas et al., 2014b):

$$n = n(E) = k \times FWHM(E), \tag{6}$$

where $k = 2.548$ for a 99.73% peak area coverage.

2.4. MC simulation

Monte Carlo technique is a powerful tool for simulations of radioactive particle transport. In this work, the background spectrum of the HPGe detector and the efficiency calibration of the double detector system were performed using a MC N-Particle transport code system (MCNP) (X-5 Monte Carlo Team, 2003). Fig. 2 shows the calculation models of the two detectors.

Sphere volumetric sources were used to simulate the radioactive background of the HPGe detector, in which γ photons flew randomly and interacted with the detectors. Natural gamma radioactive nuclides and artificial gamma radioactive nuclides were distributed uniformly within 20 km (evacuation radius) around the Fukushima Daiichi nuclear plant. Table 1 shows the main radioactive nuclides and respective activities.

Efficiency calibration of the HPGe detector was performed with surface geometry, and the spectra could be obtained directly through the pulse height tally (F8). Efficiency calibration of the $LaBr_3$ detector was performed with spherical geometry, and the density of the counts for each air volume remained constant. Every point of each efficiency curve was calculated separately by considering a monoenergetic radiation source (in the range of 50–1800 keV).

In addition, during the simulation of the sphere geometry, the secondary source method was set to reduce the variance in the simulation results, because of the source term sizes were relatively large. Generally, the secondary method included four steps:

Firstly, a sphere with a radius of 15 cm was set around the detectors. Gamma rays emitted from radioactive materials inside the spherical shell (ranging from 15 cm to R m) could be recorded as the integrated current over the sphere surface with a radius of 15 cm using the surface crossing tally (F1). Secondly, the gamma particles flux incident to the sphere surface with a radius of 15 cm was used as the secondary source to obtain the pulse amplitude spectrum of the sphere source using the pulse height tally (F8). In other words, the particles flux obtained according to the surface crossing tally (F1) were equivalent to the particles flux of the spherical shell from 15 cm to R m. Thirdly, the gamma rays emitted from radioactive materials inside the sphere with a radius of 15 cm were recorded using the pulse height tally (F8) to obtain the pulse amplitude spectrum. Finally, the total pulse height distribution was obtained by summing up the detection counts of the sphere surface with the radius of 15 cm and the detection counts of the sphere with a radius of 15 cm.

In this research, there were mainly two aspects to result in the uncertainties in MC simulation. One was the simulation method (Type A uncertainties) and the other one was the simulation model (Type B uncertainties). Further, the simulation method contained two parts uncertainties: the uncertainties in the simulations of efficiency calibration of the HPGe detector (surface geometry) and the uncertainties in the simulations of efficiency calibration of the $LaBr_3$ detector and the radioactive background of the HPGe detector (secondary source method). For simulation model, the materials and dimensions in the MC models of the HPGe and $LaBr_3$ detectors were all in accordance with the manufacturers.

3. Results

3.1. Efficiency calibration of the double detector system

The efficiency curves of HPGe and $LaBr_3$ are shown in Figs. 3 and 4, respectively. The data points in the figures are the simulated values of different γ-ray energies, in which the solid lines represent the fitting curves of the simulated efficiency, and the fitting formula is expressed as follows:

$$\ln \varepsilon_X = a_1 + a_2 E + a_3 \frac{\ln E}{E} + \frac{a_4}{E} + \frac{a_5}{E^2} + \frac{a_6}{E^3}, \tag{7}$$

where E is the specific ray energy; and a_1, a_2, a_3, a_4, a_5, and a_6 are fitting parameters. In addition, MCNP simulation results showed that the statistical errors were less than 5%.

3.2. MDAC of the double detector system

3.2.1. Source term size

The variation in source term sizes causes background alteration of the HPGe detector. The background spectra of the HPGe and $LaBr_3$ detectors are shown in Figs. 5 and 6. Meanwhile, the statistical errors about the results obtained through MCNP simulation were less than 5%.

In this article, MDAC values of some radionuclides were calculated for the dominating energy. Using 364 keV (^{131}I) and 662 keV (^{137}Cs) as examples, the MDAC variations of the double detector system with the different source term sizes are shown in Figs. 7 and

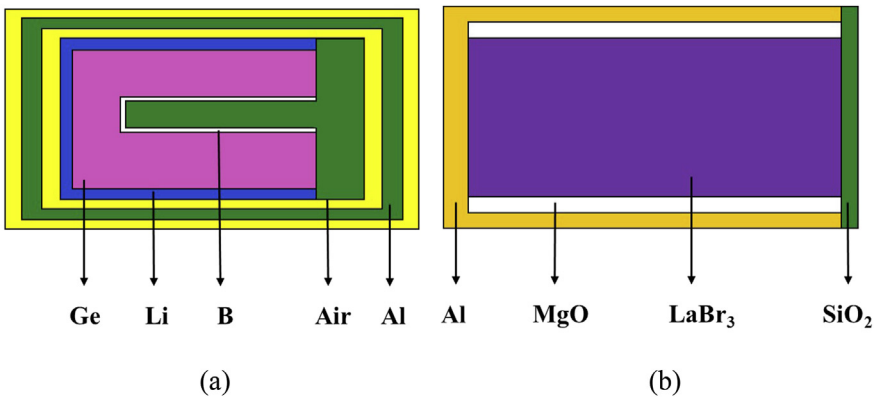

Fig. 2. Calculation models of the two detectors: (a) the HPGe detector and (b) the $LaBr_3$ detector.

Table 1
Main radioactive nuclides and activities after the Fukushima nuclear accident (http://japan.kantei.go.jp, 2011).

Radioactive nuclide	Activity (Bq)	Radioactive nuclide	Activity (Bq)	Radioactive nuclide	Activity (Bq)
^{133}Xe	1.1×10^{19}	^{127m}Te	1.1×10^{15}	^{131}I	1.6×10^{17}
^{134}Cs	1.8×10^{16}	^{129m}Te	3.3×10^{15}	^{133}I	6.8×10^{14}
^{137}Cs	1.5×10^{16}	^{131m}Te	9.7×10^{13}	^{135}I	6.3×10^{14}
^{89}Sr	2.0×10^{15}	^{132}Te	7.6×10^{14}	^{127}Sb	6.4×10^{15}
^{140}Ba	3.2×10^{15}	^{239}Np	7.6×10^{13}	^{129}Sb	1.6×10^{14}

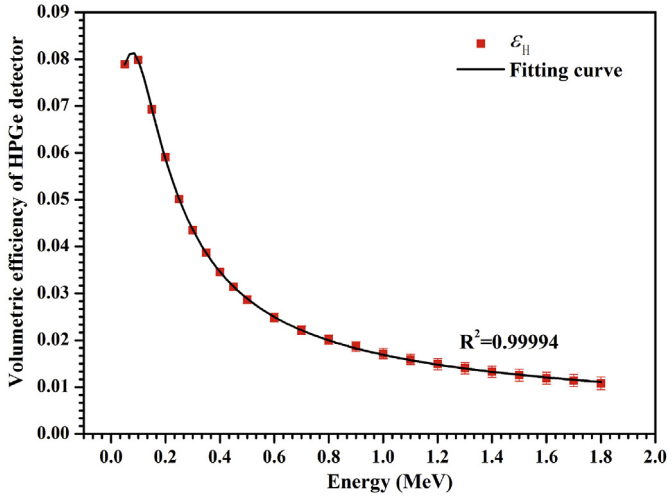

Fig. 3. Volumetric efficiency calibration fitting curve of the HPGe detector.

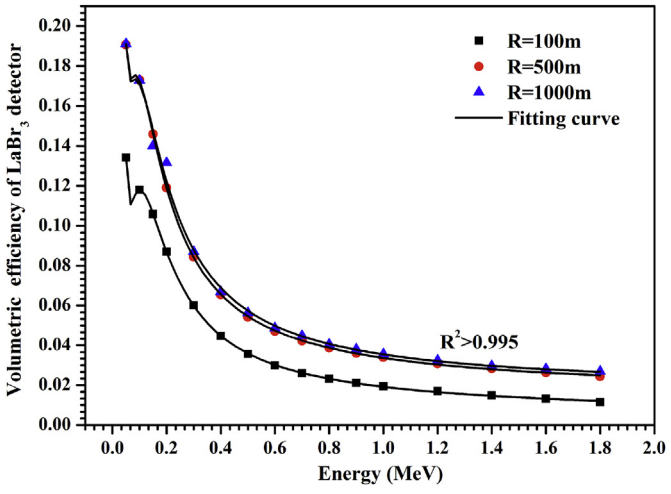

Fig. 4. Volumetric efficiency calibration fitting curves of the $LaBr_3$ detector with different detection radii (100, 500, and 1000 m).

8.

As shown in the figures, the variation in the MDAC values of the HPGe detector increased with the source term size, whereas the variation in the MDAC values of the $LaBr_3$ detector decreased with the source term size. The MDAC of both detectors exhibited saturated values when the source term sizes were large enough. Specifically, both detectors possess detection blind areas. For the HPGe detector, a larger detection radius in the air causes weak detection capability. By contrast, for the $LaBr_3$ detector, a smaller detection radius in the air indicates weak detection capability. This characteristic of NH-UAV may lead to fewer types of radionuclides being reliably detected.

The constant MDAC values can be explained by the concept of effective radius. The γ-rays that are sufficiently far away can barely reach and interact with the detector crystal. Thus, the radionuclides out of radius R_{eff} in the air are deemed to contribute no counting for the detector system, and the effective radius relates to the initial ray intensity I_0 and ray intensity through the R_{eff} thickness of air I, which can be calculated by Bagatelas et al. (2010):

$$I = I_0 e^{-\mu(E)R_{eff}}, \tag{8}$$

where $\mu(E)$is the total attenuation coefficient.

In this work, the highest energy of the γ-rays in the source term was 1.791 MeV, and the linear attenuation coefficient of the γ-rays in the air was 6.14361×10^{-3} m^{-1}. According to Equation (8), when the detection radius is larger than 1000 m, the photon number that reaches the detector is less than 0.3%. Therefore, a 1000 m detection radius can be used to simulate the infinite air environment.

The MDAC values of the detection system in the infinite air environment are shown in Table 2, which shows that the HPGe

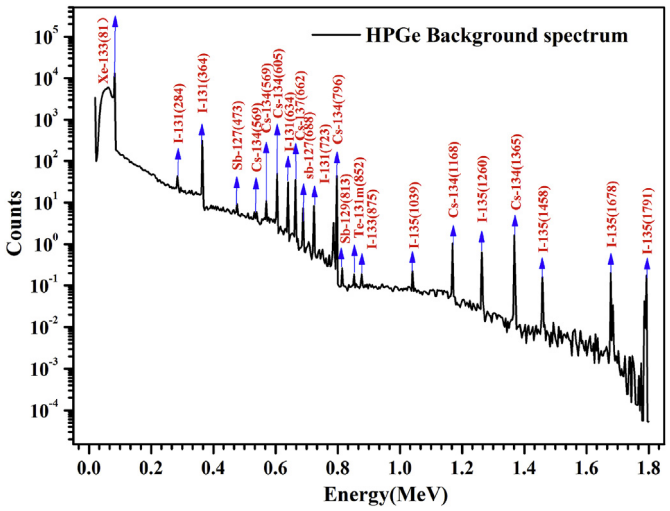

Fig. 5. Background spectrum of 1000 m detection radius of the HPGe detector.

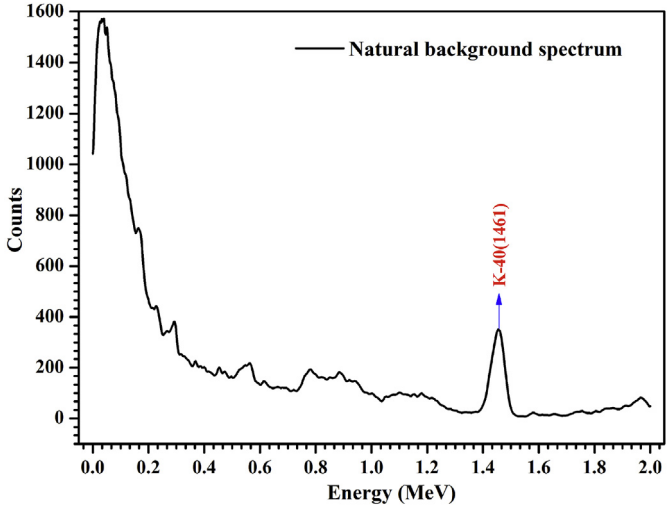

Fig. 6. Experimental background spectrum of the $LaBr_3$ detector taken in the IINT with a measuring time of 10 min.

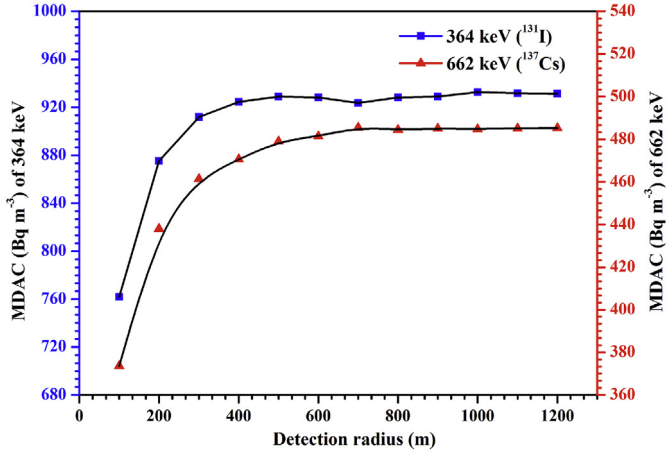

Fig. 7. Variation in the MDAC values with the different source term sizes of 364 keV (^{131}I) and 662 keV (^{137}Cs) of the HPGe detector.

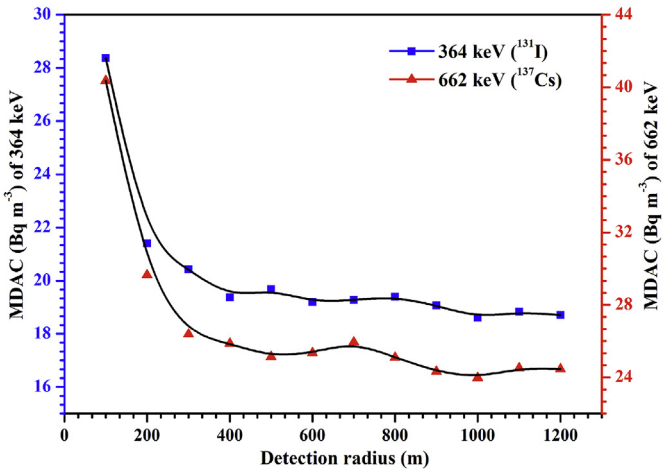

Fig. 8. Variation in the MDAC values with the different source term sizes of 364 keV (^{131}I) and 662 keV (^{137}Cs) of the $LaBr_3$ detector.

detector could detect 364 keV (^{131}I) and 605 keV (^{134}Cs), and the $LaBr_3$ detector could detect numerous radionuclides, such as 81 keV (^{133}Xe), 364 keV (^{131}I), 605 keV (^{134}Cs), 662 keV (^{137}Cs) and 686 keV (^{127}Sb).

3.2.2. *Shielding of the HPGe detector*

In the double detector system, without the shield of the HPGe detector, it is hard to distinguish between airborne radioactivity concentrations measured in the filters and the ambient air radioactivity concentrations. Moreover, the ambient radioactivity could contribute to the background detected in the HPGe and raise the MDAC in the filter measurements. Hence, installing a collimator for the HPGe detector is necessary. Meanwhile, the MDAC values can also provide data to support the shield design. The MDAC variations in the HPGe detector shielded by different thicknesses of wolfram, wolfram-nickel alloy, and lead are shown in Figs. 9 and 10. MCNP simulation results showed that the statistical errors were less than 5%.

Fig. 9 shows that the MDAC values of wolfram-nickel alloy and lead are almost same in different shield thicknesses, and the MDAC values of wolfram is lower when the shield thickness is less than 2 cm. Fig. 10 shows that in different shield thicknesses, the MDAC values of wolfram are minimum, the MDAC values of wolfram-nickel alloy are in the middle, and the MDAC values of lead are maximum. This can be explained by the HVLs of the three materials. For 364 keV rays, the HVLs of the three materials are approximately 0.16, 0.23, 0.22 cm for wolfram, lead, and wolfram-nickel alloy, respectively. For the 662 keV rays, the HVLs of the three materials are approximately 0.32, 0.74, 0.44 cm for wolfram, lead and wolfram-nickel alloy, respectively.

Besides, the obtained results showed that increasing the thickness of the shielding within a certain range effectively improved the detection capability, however, the detection capability of the HPGe detector could not be improved much when the shield thickness was greater than 4 cm. Table 3 shows the partial MDAC values of the HPGe detector shielded by 4 cm wolfram, lead and wolfram-nickel alloy.

As shown in Table 3, 4 cm wolfram exhibited optimal shielding performance among the three types of materials. For 364 keV (^{131}I) and 662 keV (^{137}Cs), the detection capability were improved by 7.24% and 20.66%, respectively.

When choosing the shield, the shielding effect usually comes first. However, other factors, such as installation convenience and

Table 2
MDAC values of the detection system for each dominating energy (in keV) of some radionuclides in the infinite air environment.

Energy (Nuclide)	Activity concentration (Bq m^{-3})	MDAC values (Bq m^{-3})	
		HPGe	$LaBr_3$
81 (^{133}Xe)	328,000.00	None	224.78
364 (^{131}I)	4774.65	957.53	18.62
605 (^{134}Cs)	537.15	510.79	20.02
662 (^{137}Cs)	447.62	502.13	23.98
686 (^{127}Sb)	190.99	710.69	55.97
813 (^{129}Sb)	4.77	180.47	60.12
852 (^{131m}Te)	2.89	316.69	98.71
1260 (^{135}I)	18.80	378.34	74.52

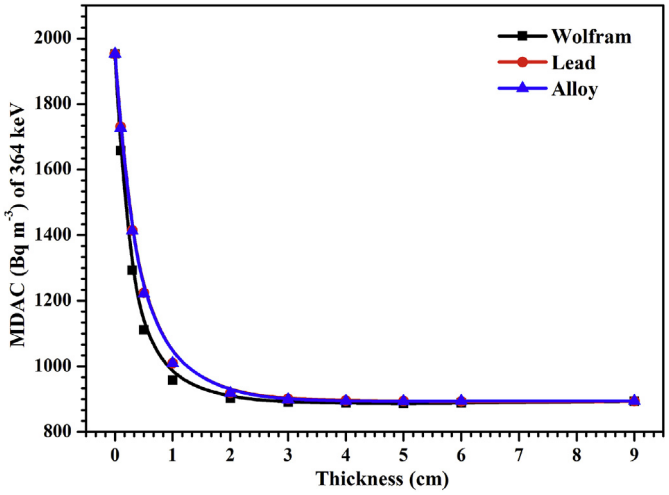

Fig. 9. Variations in the MDAC values at different thicknesses of wolfram, lead and wolfram-nickel alloy of 364 keV (^{131}I).

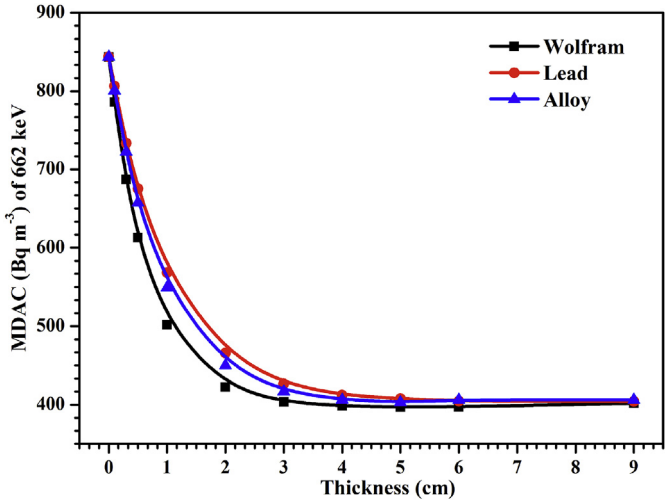

Fig. 10. Variations in the MDAC values at different thicknesses of wolfram, lead and wolfram-nickel alloy of 662 keV (^{137}Cs).

possibility of moving, should be considered, especially for the limited payload ability of NH-UAV.

3.2.3. Measuring time

Extending the acquisition time is one of the most effective means to improve the detection performance of the system. To assist users in choosing a suitable measurement time for the detection system, the relationships between the MDAC values and acquisition time for both detectors were studied. The equations for the HPGe [Equation (9)] and $LaBr_3$ detectors [Equation (10)] were deduced as follows:

$$MDAC(t) = \frac{A}{t^2} + Bt^{-1.5}, \quad (9)$$

$$MDAC(t) = \frac{C}{t} + Dt^{-0.5}, \quad (10)$$

where t is the acquisition time; and A, B, C, and D are all constants.

For the HPGe detector, given that the acquisition time is related to the volume of air (passing through the filter), the improvement in detection performance of the HPGe detector was more obvious than that of the $LaBr_3$ detector. The MDAC values of both detectors with 10 min acquisition time are shown in Table 4.

As shown in Table 4, most of the energies could be detected reliably by the detection system after the acquisition time was increased to 10 min.

Table 3
MDAC values of the HPGe detector for each dominating energy (in keV) of some radionuclides when the shield are 4 cm wolfram, lead, and wolfram-nickel alloy.

Energy (Nuclide)	MDAC values (Bq m^{-3})		
	Wolfram	Lead	Alloy
364 (^{131}I)	888.21	895.91	894.37
605 (^{134}Cs)	411.96	424.44	420.35
662 (^{137}Cs)	398.41	412.23	406.41
686 (^{127}Sb)	538.89	564.59	554.84
813 (^{129}Sb)	137.71	149.80	141.79
852 (^{131m}Te)	229.78	252.90	243.02
1260 (^{135}I)	277.38	299.48	286.49

3.2.4. Activity concentration

In a given source term size (1000 m), the MDAC curves of radioactive aerosols on filter with different activity concentrations are shown in Fig. 11.

Evidently, denser activity concentrations in the atmospheric environment incurred larger MDAC values. The background of the HPGe detector increased with the activity concentration, which gradually reduced the detection capability. The obtained relationships between MDAC values and activity concentrations can be expressed by:

$$MDAC = ax^{0.5} + b, \quad (11)$$

where x is the activity concentration; and a and b are fitting parameters.

When the concentration of the external environment increased to a certain value, the MDAC value of the HPGe detector was less than the corresponding activity concentration, that is, the gamma-rays could be detected reliably. Moreover, 364 keV (^{131}I) and 662 keV (^{137}Cs) could be detected by the HPGe detector when the concentration of the external environment was greater than 236 and 609 Bq m^{-3}, respectively. For the $LaBr_3$ detector, firstly, in a given source term size, the background B_L remains unchanged no matter how dense the activity concentration is. Secondly, in a given V_L, the source peak, the detection efficiency ε of the $LaBr_3$ has nothing to do with the activity concentration, and then the value of ε_L is unchanged. According to the Equation (4), the MDAC of the $LaBr_3$ detector would not change with the variation in activity

Table 4
MDAC values of the HPGe and $LaBr_3$ detectors for each dominating energy (in keV) of some radionuclides with the acquisition time of 10 min.

Energy (Nuclide)	Activity concentration (Bq m^{-3})	MDAC values (Bq m^{-3})	
		HPGe	$LaBr_3$
81 (^{133}Xe)	328,000.00	None	26.18
364 (^{131}I)	4774.65	14.48	26.57
605 (^{134}Cs)	537.15	1.99	1.91
662 (^{137}Cs)	447.62	11.69	26.74
686 (^{127}Sb)	190.99	1.02	2.32
813 (^{129}Sb)	4.77	1.47	5.39
852 (^{131m}Te)	2.89	0.33	5.98
1260 (^{135}I)	18.80	0.68	6.25

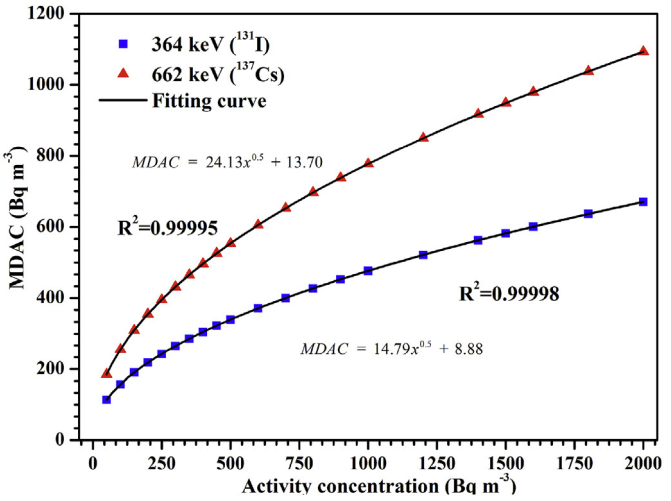

Fig. 11. MDAC values with different activity concentrations of 364 keV (^{131}I) and 662 keV (^{137}Cs).

concentration.

4. Conclusions

In this study, the MDAC of NH-UAV was calculated to assess the detection performance of the system for a priori evaluation of the measurement capability of NH-UAV by considering the Fukushima nuclear accident as research background.

In the infinite environment, the obtained results of the MDAC values showed that the HPGe detector was able to detect 364 keV (^{131}I) and 605 keV (^{134}Cs) reliably, whereas 81 keV (^{133}Xe), 364 keV (^{131}I), 605 keV (^{134}Cs), and 662 keV (^{137}Cs) were detected by the $LaBr_3$ detector. Thus, NH-UAV could be used to monitor major nuclear accidents, such as the Fukushima nuclear accident.

However, users should focus on the detection capability of NH-UAV, which could be affected by the source term size, leading to fewer types of radionuclides being detected reliably. Hence, the detection ability of the system should be improved either by prolonging the acquisition time of both detectors or increasing the shielding thickness of the HPGe detector.

For the HPGe detector, without the shield, it is hard to distinguish between airborne radioactivity concentrations measured in the filters and the ambient air radioactivity concentrations. Moreover, the ambient radioactivity contributes to the background detected in the HPGe and raises the MDAC in the filter measurements. Hence, it is necessary to install a collimator for the HPGe detector. Meanwhile, calculating the MDAC value could benefit the structure design and device optimization. When the shielding thickness reached 4 cm, the detection performance of the HPGe detector remained unchanged. Wolfram exhibited optimal detection performance among the three shielding materials. To select the appropriate shielding material for the HPGe detector, the shielding ability, installation convenience, payload capacity of NH-UAV, and other factors should be considered. Moreover, prolonging the system acquisition time also effectively enhanced system detection performance. In a specific measurement environment, users should select the appropriate measurement time according to practical needs.

In a given source term size, the detection capability of the HPGe detector was related to the activity concentration in the atmospheric environment, and the dependence was approximately MDAC $\propto$ Activity$^{0.5}$. Therefore, for a radionuclide, when its activity concentration increased to a certain value, it could be reliably detected by the HPGe detector. This finding indicated that the HPGe detector had measurement thresholds. While the MDAC of the $LaBr_3$ detector would not change with the variation in activity concentration in a given source term size.

However, this study had many limitations because the selected simulation model was too idealistic. During the simulation of air radiation monitoring, the radioactive plume was simplified using a sphere volumetric source, the detection system was assumed to be in the center of the plume, and we did not consider the ground radiation. To simulate the actual radioactive environment more realistically, in future studies, we will simulate the cases in which the NH-UAV is in different plume positions with uneven radionuclide distributions, and the radiation influence from the ground, thereby providing more reliable information of detection performance evaluation for the system to measure radioactivity in a major nuclear accident.

Acknowledgments

Xiao-bin Tang and Jia Meng contributed equally to this present work. The work was supported by the Priority Academic Program Development of Jiangsu Higher Education Institutions and the National Defense Basic Scientific Research Project (Grant No. B2520133007).

References

Airborne pods seek to trace nuclear bombs' origins http://www.sandia.gov/news/publications/LabNews/archive/12-14-12.html.
Bagatelas, C., Tsabaris, C., Kokkoris, M., Papadopoulos, C., Vlastou, R., 2010. Determination of marine gamma activity and study of the minimum detectable activity (MDA) in 4pi geometry based on Monte Carlo simulation. Environ. Monit. Assess. 165, 159–168.
Bento, J., Teles, P., Silva, L., Nogueira, P., Neves, M., Vaz, P., 2010. Performance parameters of a whole body counter. Radiat. Meas. 45, 190–195.
Cao, Y., Tang, X.-B., Wang, P., Meng, J., Huang, X., Wen, L.-S., Chen, D., 2015. Spectrum correction algorithm for detectors in airborne radioactivity monitoring equipment NH-UAV based on a ratio processing method. Nucl. Instrum. Methods Phys. Res. A 797, 290–296.
Casanovas, R., Morant, J., Salvadó, M., 2014a. Development and calibration of a real-time airborne radioactivity monitor using gamma-ray spectrometry on a particulate filter. IEEE Trans. Nucl. Sci. 61, 727–731.
Casanovas, R., Morant, J., Salvadó, M., 2014b. Development and calibration of a real-time airborne radioactivity monitor using direct gamma-ray spectrometry with two scintillation detectors. Appl. Radiat. Isot. 89, 102–108.
Castelluccio, D.M., Cisbani, E., Colilli, S., Fratoni, R., Frullani, S., Giuliani, F., 2012. SNIFFER: an aerial platform for the plume phase of a nuclear emergency. EPJ Web Conf. 24, 16–16.
Currie, L.A., 1968. Limits for qualitative detection and quantitative determination. Application to radiochemistry. Anal. Chem. 40, 586–593.
Gong, C., Zeng, G., Ge, L., Tang, X., Tan, C., 2014. Minimum detectable activity for NaI (Tl) airborne γ-ray spectrometry based on Monte Carlo simulation. Sci. China Technol. Sci. 57, 1840–1845.
http://japan.kantei.go.jp/kan/topics/201106/pdf/attach_04_2.pdf.
Khan, S., Alaamer, A.S., Tahir, S.N.A., 2008. Assessment of ^{7}Be concentration in

outdoor ambient air. Health Phys. 95, 433–435.
Kurvinen, K., Smolander, P., Pöllänen, R., Kuukankorpi, S., Kettunen, M., Lyytinen, J., 2005. Design of a radiation surveillance unit for an unmanned aerial vehicle. J. Environ. Radioact. 81, 1–10.
Lee, J.I., Kim, J., Lee, D.M., Choi, H.Y., Kim, B.J., Shin, H., 2009. Design of aircraft-carried sampling system for aerial radioactivity monitoring. Ann. Nucl. Energy 36, 133–144.
MacFarlane, J., Payton, O., Keatley, A., Scott, G., Pullin, H., Crane, R., Smilion, M., Popescu, I., Curlea, V., Scott, T., 2014. Lightweight aerial vehicles for monitoring, assessment and mapping of radiation anomalies. J. Environ. Radioact. 136, 127–130.
Peräjärvi, K., Lehtinen, J., Pöllänen, R., Toivonen, H., 2008. Design of an air sampler for a small unmanned aerial vehicle. Radiat. Prot. Dosim. 132, 328–333.
Pöllänen, R., Toivonen, H., Peräjärvi, T., Karhunen, T., Lehtinen, J., 2009. Radiation surveillance using an unmanned aerial vehicle. Appl. Radiat. Isot. 67, 340–344.
Sanada, Y., Torii, T., 2015. Aerial radiation monitoring around the Fukushima Dai-ichi nuclear power plant using an unmanned helicopter. J. Environ. Radioact. 139, 294–299.
X-5 Monte Carlo Team, 2003. MCNP – Version 5, Vol. I: Overview and Theory. LA-UR-03–1987.
Zhang, Y., Li, C., Liu, D., Ying, Z., Yan, L., 2015. Monte Carlo simulation of a NaI(Tl) detector for in situ radioactivity measurements in the marine environment. Appl. Radiat. Isot. 98, 44–48.